Mesoporous Silica Nanoparticles Decorated with Carbosilane Dendrons as Novel Nonviral Oligonucleotides Delivery Carriers

Ángel Martínez,[a,c] Elena Fuentes-Paniagua,[b,c] Alejandro Baeza,[a,c] Javier Sánchez-Nieves,[b,c] Mónica Cicuéndez,[a,c] Rafael Gómez,[b,c] F. Javier de la Mata,*[b,c] Blanca González,*[a,c] and María Vallet-Regí*[a,c]

Abstract: A novel nanosystem based on mesoporous silica nanoparticles covered with carbosilane dendrons grafted on their external surface is reported. This system is able to transport single oligonucleotide strands into cells, avoiding the electrostatic repulsion between the cell membrane and the negatively charged nucleic acids thanks to the cationic charge provided by the dendron coating in physiological conditions. Moreover, the presence of the highly ordered pore network inside the silica matrix would make possible to allocate other therapeutic agents within the mesopores with the aim of achieving a double delivery. First, carbosilane dendrons of second and third generation possessing ammonium or tertiary amine groups as peripheral functional groups were prepared. Hence, different strategies were tested in order to obtain their suitable grafting on the nanoparticles outer surface. As nucleic acid model, a single stranded DNA oligonucleotide tagged with a fluorescent Cy3 moiety was used to evaluate the DNA adsorption capacity. The hybrid material functionalized with the third generation of neutral dendron showed excellent DNA binding properties. Finally, the cytotoxicity as well as the capability to deliver DNA into cells, was tested *in vitro* using a human osteoblast-like cell line, achieving good levels of internalization of the vector DNA/carbosilane dendron functionalized material without affecting cellular viability.

Introduction

The process by which exogenous nucleic acids sequences are introduced into the interior of a cell is known as gene transfection. Nowadays the applications of gene transfection are mainly in the field of biotechnology, since gene transfection performed *in vitro* opens huge possibilities for the DNA reprogramming of bacteria and eukaryotic cells.[1] Regarding human health care perhaps the most promising application is gene therapy,[2] in which the therapeutic delivery of nucleic acids is intended to correct or modify the expression of the gene influencing a genetic disorder. Currently, gene therapy is also being developed as an alternative or complementary therapy in cancer treatment[3] and other acquired diseases, such as cardiovascular and neurodegenerative ones and some immunodeficiencies such as HIV.[4]

There are two main nucleic acid delivery approaches that are conceptually different. On the one hand, the delivery of DNA fragments into the cell nucleus to be finally expressed as the protein which it codifies for. Another alternative is gene silencing or an antisense strategy, that knockdowns gene expression of an individual gene involving antisense DNA oligonucleotides or short interfering RNA (siRNA) sequences that bind to targeted messenger RNA (mRNA) and initiate its degradation, in the nucleus or in the cytoplasm, respectively.[5]

However, the delivery of foreign nucleic acids into the interior of a cell is not an easy task and needs to overcome several biological obstacles that prevent the therapeutic delivery of DNA/siRNA. For instance, the lipid bilayer of the cell membrane acts as a biological barrier against foreign and pathogenic nucleic acids, and nuclease activity rapidly degrades nucleic acids sequences. Hence, designing effective carrier vectors for the nucleic acid delivery is one of the biggest challenges in the field of gene therapy. Vectors must be vehicles able to compact and protect oligonucleotides and to actively cross the lipid membrane, delivering nucleic acid cargos with efficiency and limited toxicity. Currently there is a research effort focused on the design of synthetic nonviral nanovectors,[6] as a safer and more biocompatible alternative to viral vectors. Based on different chemical building blocks, a broad variety of nonviral vectors have been developed from biocompatible nanostructured materials. These systems are, for example, cationic polymers, polymeric nanocapsules, liposomes, dendrimers, and inorganic nanoparticles.[7,8]

Dendrimers are globular, highly branched macromolecules with structural uniformity. Due to their multivalency they have been employed in different areas of biomedicine such as protein mimic, drug delivery agents, carriers of drugs, imaging agents, antiviral and antibacterial agents.[9,10] The potential use of dendrimers mainly depends on the peripheral groups. In order to be used as delivery systems for nucleic acids, cationic groups must be placed on periphery so dendrimers can interact with the negative phosphate groups of the nucleic acids. In this sense, dendritic molecules have been widely employed as delivery

[a] Á. Martínez, Dr. A. Baeza, Dr. M. Cicuéndez, Dr. B González, Prof. M. Vallet-Regí.
Departamento de Química Inorgánica y Bioinorgánica
Facultad de Farmacia, Universidad Complutense de Madrid
28040 Madrid, Spain.
E-mail: blancaortiz@ucm.es, vallet@ucm.es

[b] Dr. E. Fuentes-Paniagua, Dr. J. Sánchez-Nieves, Dr. R. Gómez, Dr. F. J. de la Mata
Departamento de Química Orgánica y Química Inorgánica
Facultad de Farmacia, Universidad de Alcalá
28871 Alcalá de Henares, Spain.
E-mail: javier.delamata@uah.es

[c] Á. Martínez, Dr. E. Fuentes-Paniagua, Dr. A. Baeza, Dr. J. Sánchez-Nieves, Dr. M. Cicuéndez, Dr. R. Gómez, Dr. F. J. de la Mata, Dr. B. González, Dr. M. Vallet-Regí
Networking Research Center on Bioengineering, Biomaterials and Nanomedicine (CIBER-BBN), Spain.

Supporting information for this article is given via a link at the end of the document.

systems for nucleic acids mainly against cancer or HIV.[11,12] Also, bonding of dendrimers to other molecules might allow obtaining combined properties of dendrimer and the extra molecule.[13]

On the other hand, dendrons are cone shaped hyperbranched macromolecules with the same properties of dendrimers, which possess two well differentiated regions, one with the desired functions at periphery, and other with an extra reactive moiety at the focal point. The presence of the extra reactive moiety of dendrons may allow their use in order to obtain more complex structures such as tectodendrimers,[14] dendronized polymers,[15] dendronized nanoparticles[16] or dendronized nanotubes[17] what would allow the combination of the dendritic properties with the ones of the dendronized material. Furthermore, it has been previously reported that the introduction of peptide dendrons on mesoporous nanoparticles did not influence the biocompatibility of the nanoparticles.[18] As well, dendron bearing lipids have also been used in gene transfection.[19] Recently, carbosilane dendrons have been used to prepare nanoparticles from nano-emulsions to be used as nonviral carriers for antisense oligonucleotides.[20]

Regarding inorganic nanoparticles, mesoporous silica nanoparticles (MSNs) exhibit attractive characteristics to be used in nanomedicine, such as the possibility of controlling their particle size in the 50-300 nm range, tuneable pore diameter, chance of functionalization of the silica surface, biocompatibility and large surface areas and pore volumes, which allow entrapping large amounts of cargo molecules.[21] In addition to their application for the controlled release of drugs,[22] MSNs have the potential to act as delivery platforms of genetic material. A selective surface functionalization can introduce positive charges on the silica surface, which in turn permits electrostatic interactions with negatively charged nucleic acids. In a pioneering work, the group of Lin developed a gene transfection reagent based on MCM-41-type mesoporous silica nanospheres functionalized with the second generation of PAMAM dendrimers.[23] From then, most of the studies have been focused in accomplishing targeted and dual drug and siRNA delivery from the MSNs platform to the same population of tumor cells in a coordinated manner. The sequential delivery or co-delivery of siRNA and anticancer drugs represents a combined therapy mainly aimed at overcoming drug resistance in the treatment of cancer.[24]

Recent research trends are focused on the possibility to host the genetic material inside the mesopores of the MSNs, instead of carrying it on the outer surface. The advantages brought up in this strategy are a high adsorption capacity for nucleic acids in the inner space, as well as an effective protection against nuclease enzymatic degradation. New approaches and synthetic routes to prepare MSNs simultaneously with accessible large pores (>10 nm), small particle dimensions (<300 nm) and well-ordered mesostructure have been already developed to obtain such monodispersed large pore MSNs aimed at gene delivery applications. For instance, large pore MSNs with no mesoporous order but having a high monodisperse particle size distribution of about 250 nm[25] and large pore MSNs with a 3D-cubic mesostructure have been prepared.[26,27] Recently, a facile self-assembly solvothermal strategy where the mesostructure of the resultant large pore MSNs can be easily tuned during synthesis between cubic, hexagonal and lamellar has been reported.[28] As well, other kind of silica nanomaterials with dendritic pore structures have demonstrated DNA adsorption capacity and effective *in vitro* delivery.[29]

In this work we report the functionalization of the external surface of MSNs with carbosilane dendrons of second and third generation possessing ammonium or tertiary amine groups as peripheral functional groups, via two different synthetic approaches. Carbosilane dendrons are used as biocompatible and nontoxic cationic entities to decorate nanoparticles in the search of new nonviral gene delivery systems. After detailed physic-chemical characterization of hybrid organic-inorganic materials, a single stranded DNA oligonucleotide tagged with a fluorescent Cy3 moiety (ssDNA^{Cy3}) has been used to evaluate DNA adsorption capacity of both materials, as a model for *in vitro* gene transfection of antisense DNA or siRNA oligonucleotides. Then, *in vitro* cell studies have been carried out in a human osteoblast-like cell line (HOS) to evaluate levels of nanomaterials cell uptake, cytotoxicity and DNA internalization ability of the dendron functionalized MSNs.

Results and Discussion

Carbosilane dendrons were selected to functionalize the external surface of mesoporous silica nanoparticles for two main reasons. On one hand, the carbosilane dendritic framework is expected to have a better interaction with the cell membrane since it is lipophilic. On the other hand, the possibility to reduce the steric hindrance at the silica surface, since the reactive focal point is less congested in dendritic wedges in contrast to dendrimers. In addition, this family of carbosilane dendrons offers the possibility to have cationic and neutral amine terminal groups, as well as different functional groups at the periphery and the focal point, which is a great advantage for synthetic purposes.[30,31]

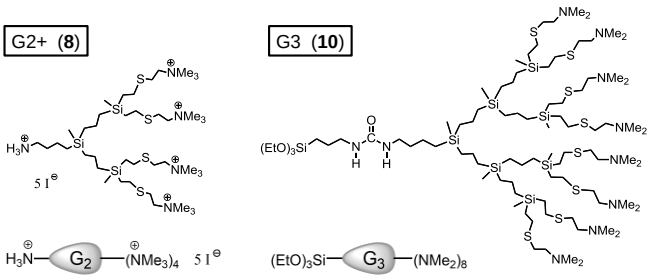

Chart 1. Carbosilane dendrons used for the functionalization of MSNs.

To proceed with hybrid materials preparation, carbosilane dendrons (Chart 1) and mesoporous silica nanoparticles were independently synthetized, so that the grafting of dendrons to the silica support is performed via a post-synthesis method. In this way the organic part to be coupled to the silica surface can be accurately characterized. We used two different synthetic

approaches for the covalent attachment of cationic and neutral carbosilane dendrons to the MSNs external surface: *i)* a two-step functionalization route, in which the external surface of the MSNs is first provided with carboxylic acid groups and, in a second reaction step over the mesoporous material, the cationic **G2+** dendron is anchored via a condensation reaction between primary amines of the focal point and the carboxylic acids (Scheme 1) and *ii)* a straight functionalization route, in which the covalent attachment of the carbosilane dendron to the silica surface is performed via a condensation reaction with silanol groups (Scheme 2) and therefore, a reactive alkoxysilane function is previously introduced into the focal point of dendron **G3**. With these two different synthetic approaches we are trying to obtain comparable nanosystems, possessing the carbosilane dendrons anchored in the outer surface of MSNs having their free inner mesopores channels with their intact silanol surface.

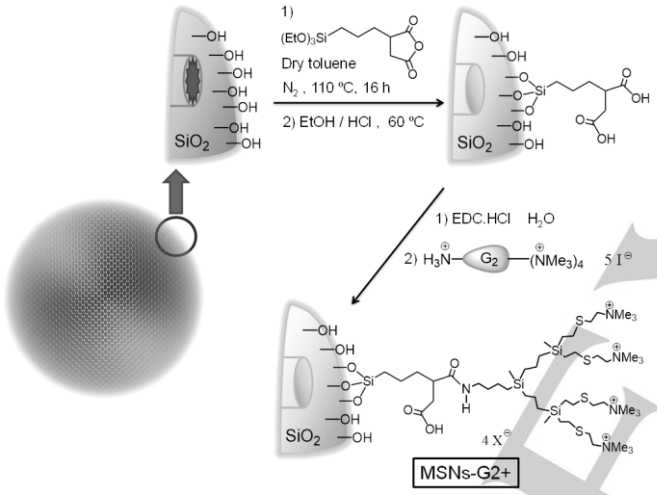

Scheme 1. Two step functionalization of MSNs with $H_3N^+G_2(N^+Me_3)_4$ (**8**) dendron. The colour version of this figure is available in the Supporting Information for this article.

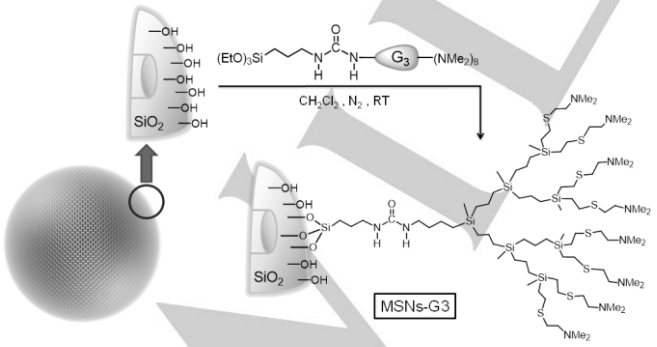

Scheme 2. Straight functionalization of MSNs with $(EtO)_3SiG_3(NMe_2)_8$ (**10**) dendron. The colour version of this figure is available in the Supporting Information for this article.

Synthesis and characterization of carbosilane dendrons

In order to obtain carbosilane dendrons with a primary amine group at the focal point and cationic $-NMe_3^+$ groups in their periphery (Scheme 3), we have used as precursors the cationic carbosilane dendrons $PhtG_n(NMe_2{\cdot}HCl)$ previously reported.[30] The nomenclature employed for dendrons in this paper is of the type XG_nY_m, where X indicates the focal point of the dendron, G_n generation and Y_m the peripheral functions (Y) and its number (m). To synthesize the required cationic dendrons $NH_3^+G_n(NMe_3^+)_m$, we firstly neutralized dendrons $PhtG_n(NMe_2{\cdot}HCl)$, then the amine groups were quaternized with MeI, and finally the focal point was deprotected. All these compounds were obtained with good yields (over 80 %).

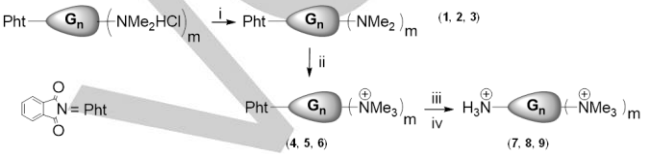

Scheme 3. Synthesis of cationic dendrons. $PhtG_n(NMe_2HCl)_m$ starting compounds were synthesized as previously published.[30] *i)* Na_2CO_3, *ii)* MeI; *iii)* N_2H_4, *iv)* HI.

The dendrons $PhtG_n(NMe_2{\cdot}HCl)$ (n = 1, m = 2; n = 2, m = 4; n = 3, m = 8) were neutralized by addition of an excess of Na_2CO_3, obtaining the corresponding amine dendrons $PhtG_n(NMe_2)_m$ (n = 1, m = 2 (**1**); n = 2, m = 4 (**2**); n = 3, m = 8 (**3**)) as pale yellow oils soluble in a variety of organic solvents, ethers, halogenated solvents, alcohols, DMSO, etc, but not in water. In general, the NMR data were very similar to those obtained for the parent compounds.[30] The main differences were those related with the chemical change in the N atoms. In the ^{1}H NMR spectra, the NMe_2 and CH_2N groups were shifted to lower frequencies, δ *ca.* 2.20 and 2.45 respectively. In the ^{13}C NMR spectra the C atoms of these groups were observed at δ *ca.* 45.2 and δ *ca.* 59.1 respectively, whereas the chemical shift of the N atoms in the ^{1}H-^{15}N NMR spectra was detected at δ *ca.* -353.1.

Afterwards, addition of excess MeI to dendrons **1-3** afforded the cationic derivatives $PhtG_n(NMe_3^+)_m$ (n = 1, m = 2 (**4**); n = 2, m = 4 (**5**); n = 3, m = 8 (**6**)) as white solids soluble in water, alcohols and DMSO. The presence of the ammonium functions was confirmed in the ^{1}H NMR spectra by the shifting to higher frequencies of the resonances corresponding to the methyl substituents of the NMe groups over δ 3.10, as well as the methylene groups CH_2N over δ 3.53. A similar effect is observed in the ^{13}C NMR spectra where these peaks appear about δ 52 and 63.8. The chemical shift corresponding to these N atoms was observed at δ *ca.* -330, as consequence of the presence of the positive charge on the nitrogen atom.

Finally, excess of hydrazine, to remove the protecting phtalimide group and transform it into a primary amine, and HI, to purify properly the new compounds, were added, obtaining the cationic dendrons $NH_3^+G_n(NMe_3^+)_m$ (n = 1, m = 2 (**7**); n = 2, m = 4 (**8**); n = 3, m = 8 (**9**)), which were obtained as pale yellow

solids soluble in water, alcohols and DMSO. The transformation of the focal point was confirmed in the ^{1}H NMR by the disappearance of the aromatic protons and by the shifting of the resonance of the corresponding NCH_2 from δ *ca.* 3.55 to δ *ca.* 2.78 in compounds **7**-**9** (see Figure 1 for compound **8**). Additionally the resonance corresponding to the $–NH_3^+$ protons could be observed at approximately 7.6 ppm as a broad signal ($[D_6]$DMSO). The change at the focal point could also be observed in the $\{^{1}H\text{-}^{13}C\}$ HSQC spectra were the resonance corresponding to the group NCH_2 could be observed at δ *ca.* 38.4 (see Figure S5 for compound **8**). Finally, the chemical shift corresponding to this N atom was shifted from -217.7 in the phthalimide derivatives to -346.3 ppm in the free ammonium **7**-**9**.

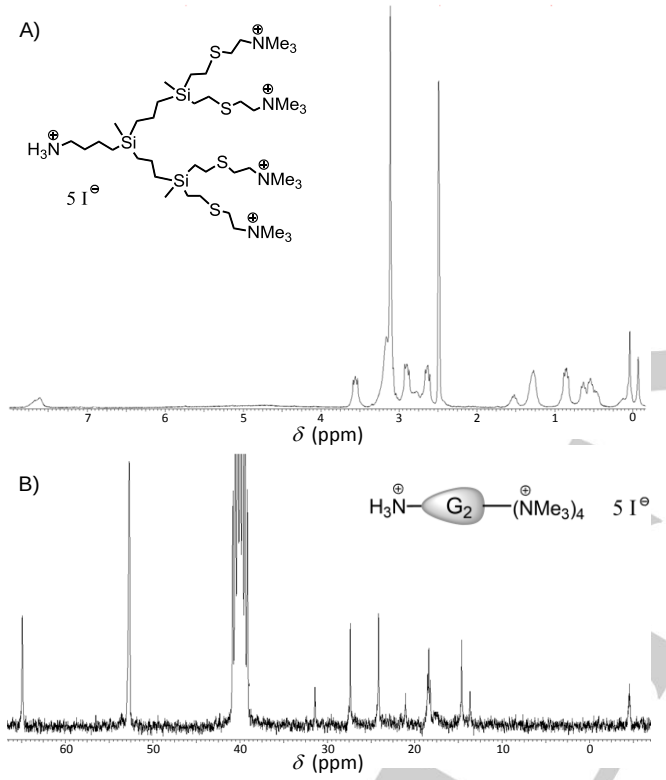

Figure 1. A) ^{1}H NMR ($CDCl_3$) and B) ^{13}C NMR ($CDCl_3$) for cationic dendron **$H_3N^+G_2(N^+Me_3)_4$** (**8**).

Synthesis of carbosilane dendron $(EtO)_3SiG_3(NMe_2)_8$

For the covalent grafting of dendron wedges onto the silica surface in a direct attachment we have introduced a reactive silyl function such as $–Si(OR)_3$ into the focal point of the dendron. The alkoxysilane group allows the dendrons to bond covalently to the silica surface of the MSNs via postsynthetic grafting. Therefore, a reactive triethoxysilane moiety was coupled to the focal point of dendron **$H_2NSiG_3(NMe_2)_8$** through the well-known reaction of primary amines with isocyanates (Scheme 4). This reaction forms the chemically stable urea group and, as a rule, gives no by-products and often occurs at room temperature in quantitative yields. Compound **$(EtO)_3SiG_3(NMe_2)_8$** (**10** or **G3**) (Chart 1) was synthesized at room temperature in dry CH_2Cl_2 under argon atmosphere, using equimolar amounts of 3-isocyanatopropyltriethoxysilane and the third generation of neutral dendron with $-NH_2$ group at the focal point. However, for the grafting reaction with the silica surface, a slight molar defect of 3-isocyanatopropyltriethoxysilane with respect to the amine group in the focal point of the dendron was used. Assuming that unfunctionalized **G3** dendron would not graft the silica surface, we avoid in this way possible unreacted 3-isocyanato-propyltriethoxysilane to be present in the grafting reaction. This possibility would lead to undesired groups from the hydrolyzed isocyanatopropyl groups onto the silica surface.

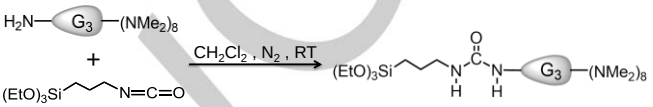

Scheme 4. Alkoxysilane derivatization of dendron $H_2NG_3(NMe_2)_8$ in the focal point.

Urea moiety formation and termination of the reaction was verified by means of FT-IR spectroscopy. The strong and sharp absorption band at 2272 cm^{-1}, attributed to the vibration of the isocyanate group (–N=C=O), disappeared shortly after addition. Structural characterization of **G3** dendron silylated at the focal point was achieved by ^{1}H, ^{13}C and ^{29}Si NMR spectroscopies and MALDI-TOF mass spectrometry (Figures S7-S10).

The $^{13}C\{^{1}H\}$ NMR spectrum reveals a singlet at 158.6 ppm which is attributed to the new carbonyl group of the spacer fragment. The ^{29}Si NMR spectrum shows three signals at 1.94, 1.54 and 0.91 ppm that correspond to the silicon atoms situated at different generation levels of the dendron framework. In addition, a single resonance in the region of the T-type silicon atoms turns up at –45.4 ppm, and it is assigned to the silicon atom able to undergo sol-gel chemistry. As only one signal appears, the existence of a single silicon type is confirmed, which means that the introduced function, *i.e.*, the triethoxysilane group, remains unchanged and is ready to be used in the next step of grafting to the mesoporous silica. MALDI-TOF mass spectrum shows a peak at *m/z* 1931.96 with isotopic pattern matching exactly the calculated value for the protonated dendron.

MSNs materials synthesis

Green emitting fluorescent mesoporous silica nanoparticles (**MSNs**) were prepared in a two steps process, following previously reported procedures.[32-34] The fluorescent dye is covalently linked to the silica network, making the MSNs traceable by flow cytometry and fluorescence microscopy for the *in vitro* cell studies. Fluorescein isothiocyanate was first reacted with 3-aminopropyl-triethoxysilane and the *in situ* generated intermediate was then co-condensed along with TEOS in a base-catalyzed sol-gel process at high temperature in the presence of CTAB as structure directing agent. The synthesized MSNs had uniform morphology and highly ordered mesostructures. The scanning electron micrographs (Figure

S11) reveal that the MSNs are spherical in shape with an average diameter of *ca*. 200 nm. The MCM-41 type mesoporous structure was analyzed by nitrogen sorption measurements, having a 2.71 nm average pore diameter and a surface area of 997.1 m^2g^{-1}, and further confirmed by powder X-ray diffraction (XRD). The small angle XRD pattern of the MSNs shows a well resolved characteristic profile of MCM-41 materials, indicating that the starting MSNs material used for the preparation of hybrid materials has a well ordered mesopores network with a lattice spacing of 3.78 nm.

Dendron grafting to mesoporous silica

The post-synthesis grafting sol-gel reactions were carried out under water free conditions in order that the distribution of organic molecules is constrained by the surface silanol groups and to avoid self-condensation of alkoxysilane precursors in the presence of water.[35] The required amount of alkoxysilane derivative was calculated to achieve a maximum coverage of the external nanoparticle surface, *i.e.*, a 100% nominal degree of surface functionalization, plus a 10% excess. Therefore, it was taken into account the specific surface area of the isolated powder materials, of which approximately a quarter was estimated to correspond to the external surface. We took into account the stoichiometry of the condensation reaction between the free silanol groups of the silica exterior surface and the alkoxysilane functionalized derivatives in a molar ratio of three Si–OH with one R-Si$(OEt)_3$. Also, it was assumed that the average surface concentration of Si–OH in amorphous silica materials is 4.9 $OHnm^{-2}$, as was estimated by Zhuravlev.[36]

To prepare MSNs with carboxylic acid groups only on the external surface (**MSNs-COOH$_{ext}$**), the post-grafting reaction of the succinic anhydride organosilane TESPSA was conducted on the as-synthetized material containing surfactant templates filling the pores.[37] It is known that by performing the postgrafting of template filled MSNs, diffusion of silane coupling reactant into the porous structure is limited thus leading to a preferential functionalization of the outer surface.[38] Removal of the CTAB surfactant template was then performed using acidified methanol as extracting solution to attain in the same step the anhydride ring opening which affords the carboxylic acid groups.

Steric and electrostatic hindrance plays a key role in the case of dendritic functionalization of silica surfaces, and this effect is more pronounced for higher generations. Therefore, we can expect that a maximum surface coverage is achieved and beyond this limit the inorganic support surface is essentially blocked and therefore, even though anchoring points are available, there is no space for more dendrimers to reach them.[39] The electrostatic effect should be indeed even more pronounced in the case of the cationic **G2+** dendritic wedge. For that reason, a study of the required amount of **G2+** dendron was firstly made, to optimize the enough quantity to enter the maximum amount of organic matter, avoiding at the same time wasting dendritic wedges. Three different stoichiometries of dendron per nominal –COOH group were assayed, 1 eq (100%), 1/4 eq (25%) and 1/16 eq (6.25%), obtaining no significant differences in the amount of **G2+** dendron incorporated to the nanoparticles (See TG and AQE data in Table 1). This finding is consistent with the high electrostatic repulsion produced among polycationic dendrons, and from this fact we used the lower stoichiometry to prepare **MSNs-G2+** material. In this line, taking into account the possibility that carbosilane dendrons of third generation hardly reach the interior of the MCM-41 pores, together with the expected steric hindrance at the time to react with the silica surface, we established a nominal degree of surface functionalization for **MSNs-G3** material, calculating the amount of dendron needed to functionalize the 25% of the external surface of the nanospheres.

Table 1. Organic content and sulphur composition from thermogravimetric and chemical analysis of MSNs and functionalized MSNs materials.

Sample	Theor. Org. (wt%)	Org. content (wt%) [a]	%S
MSNs	---	4.9	0.04
MSNs-$COOH_{ext}$	9.0%	12.0	0.02
MSNs-2G+ (100%)	67.9%	20.0	0.41
MSNs-2G+ (25%)	37.9%	22.3	0.31
MSNs-2G+ (6.25%)	18.5%	21.9	0.38
MSNs-3G	23.0%	19.8	3.67

[a] Organic content (wt%) is determined from the TGA weight losses, excluding the weight loss due to the desorption of water (up to 125 ºC) and further corrected by the weight loss of the surfactant extracted unmodified fluorescent MSNs.

The organic content of the hybrid MSNs materials was determined from thermogravimetric analyses and the sulphur elemental composition was measured to easily follow the incorporation of **G2+** and **G3** dendrons (Table 1). As above commented, the lower stoichiometry used for the functionalization with the cationic **G2+** dendron is enough to achieve the maximum dendron load, since sulphur quantity and organic matter remain in similar values for all **MSNs-G2+** samples. In all **MSNs-G2+** samples the organic matter is due to the alkoxysilane previously incorporated in the first reaction step plus the **G2+** dendron attached in the second one. Unlike in **MSNs-G2+**, organic content measured in **MSNs-G3** material comes exclusively from the dendron, which is also reflected in the sulphur quantity. Therefore, the straight functionalization route with **G3** dendron appears to be more effective to achieve a bigger dendron load, not surprisingly consistent with the high electrostatic repulsions occurring in **G2+** but not in **G3** dendron, being the latter a higher generation but neutral charged.

Figure 2 shows the ^{1}H HRMAS NMR spectrum of the nanoparticles modified with **G3** carbosilane dendron, together with the solution ^{1}H NMR spectrum of the free dendritic sol-gel precursor **$(EtO)_3SiG_3(NMe_2)_8$**. The presence of the **G3** dendron on the nanoparticles surface is supported by the chemical shifts of the hybrid material, which closely match those of the respective functional groups in the solution NMR spectrum of the free compound.[40] In general, the spectral features of the hybrid material are broad signals that appear slightly down field shifted

with respect to the carbosilane dendron in solution. The broadening of signals is normal since the organic matter is indeed immobilized onto the solid nanoparticles. For the chemical shifts it must be taken into account the use of different deuterated solvents used to perform the measurements, as well as differences in technique and equipment. Although signals due to ethoxy groups still remain in the **MSNs-G3** spectrum (shoulder at *ca.* 1.30 and 3.73 ppm), their relative area decrease quite a lot, demonstrating that the hydrolysis of the alkoxysilane derivative takes place in a high extent. Condensation with Si-OH groups onto the silica surface can be determined with the ^{29}Si MAS NMR study confirming the covalent attachment, as discussed below.

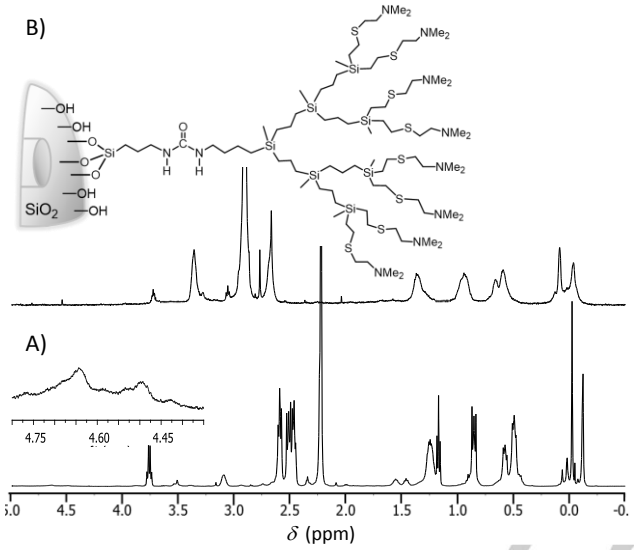

Figure 2. A) ^{1}H NMR spectrum ($CDCl_3$) of dendron **$(EtO)_3SiG_3(NMe_2)_8$** (**10**) (inset: expansion of the δ zone where N*H*CON*H* signals appear). B) ^{1}H HRMAS NMR spectrum (suspension in D_2O) of **MSNs-G3** material.

A remarkably fact due to the measurement of **MSNs-G3** in D_2O suspension, is that signals from methyl and methylene groups adjacent to the terminal tertiary amines experience a large shift to lower field compared to the $CDCl_3$ solution spectrum. This is due to the protonation of the tertiary amines that takes place in water, introducing a positive charge on the N atom and, therefore, unshielding the nearby protons. The peak from methyl groups in the precursor, $–CH_2N(CH_3)_2$, are shifted from 2.23 to 2.91 ppm in the hybrid material in D_2O. As well, the methylene groups, $–CH_2N(CH_3)_2$, suffer a big shift, from 2.47 to 3.37 ppm. In a similar way, a smaller shift occurs for the signal from the methylenes adjacent to the urea group, from 3.10 to 3.29 ppm. This observed protonation clearly explains that the **MSNs-G3** material is able to complex nucleic acids in water media, without the needing of a methylation reaction to provide the material with permanent positive charges. Due to a polyelectrolyte effect in dendrimers,[41] the pK_a of these tertiary amines must be lower than the pK_a of similar amines, such as Et_3N (pK_a = 10.8), but still enough for the protonation to take place, rendering the nanoparticles sufficient positive charge for nucleic acid complexation in water.

The $^{13}C\{^{1}H\}$ CP MAS NMR spectrum of **MSNs-G2+** (Figure 3.A) indicates the covalent attachment of dendron **G2+** to the surface of **$MSNs\text{-}COOH_{ext}$**. In addition to the carbonyl signal at 177 ppm, due to the carboxylic acid groups of the **$MSNs\text{-}COOH_{ext}$** material, a new signal at 158 ppm shows up, confirming the formation of an amide functional group (NHCO). As expected from TG and AQE data, only a low proportion of –COOH are converted to amide groups, so the high excess of free carboxylic acid group attached on the mesoporous surface clearly presents a resonance in this spectrum, since the organic matter that comes from the dendron in this sample is lower than the theoretical. Figure 3.B shows the $^{13}C\{^{1}H\}$ CP MAS NMR spectrum of **MSNs-G3**, which proves that the organic matter present in the nanoparticles indeed corresponds to the **G3** dendron, since the observed ^{13}C chemical shifts closely matched those of respective functional groups in the solution NMR spectra of the silylated free compound. A distinct peak attributed to the carbonyl carbon of the urea group (NHCONH) is observed at 162 ppm, although since the urea functional group is considerably less abundant in the **G3** dendron, this carbon atom gives rise to a very weak signal. Methylene carbons directly attached to nitrogen atoms (CH_2N) show a peak at 59 ppm. The peak at *ca.* 45 ppm corresponds to the sum of methyl carbons next to the terminal amine groups (NMe_2). Methylene carbons adjacent to the sulphur atom of the dendrimer framework (CH_2S) show a peak at 29 ppm, and those adjacent to the silicon atom at 20 ppm. The peak at *ca.* -3 ppm is due to the methyl groups bonded to the silicon atom (CH_3Si). Comparing both spectra of dendron functionalized samples, signal due to methyl groups attached to the terminal nitrogen appears at 45 ppm for **MSNs-G3**, and approximately 10 ppm shifted to down field, at 56 ppm, for **MSNs-G2+**, due to the greater unshielding produced by the positive charge.

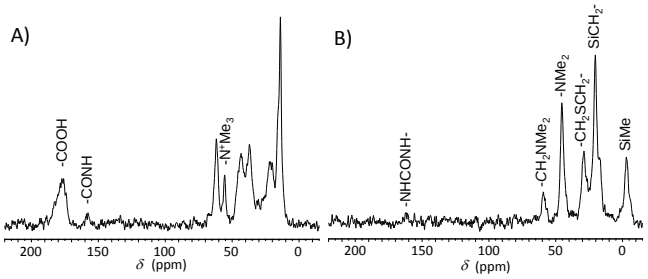

Figure 3. $^{13}C\{^{1}H\}$ CP MAS NMR spectra of A) **MSNs-G2+** and B) **MSNs-G3** materials.

Further analysis of the functionalization of mesoporous silica nanoparticles was made by solid state ^{29}Si MAS NMR spectroscopy. Figure 4 compares the quantitative spectra from the direct polarization method obtained for the bare MSNs material with those obtained for the dendron functionalized materials. Although CP experiments use cross-polarization from the nearby protons and, therefore, yield unquantitative spectra,

^{29}Si CP MAS NMR spectra were also recorded (Figure 4, top) to confirm the presence of *T* units [R–Si(OSi)$_n$(OX)$_{3-n}$] (X = H, C), which are indicative of the organosilane groups in the materials.

In all the spectra the resonances at around −93, −103, and −112 ppm represent Q^2 [Si(OSi)$_2$(OX)$_2$], Q^3 [Si(OSi)$_3$(OX)] and Q^4 [Si(OSi)$_4$] silicon sites, respectively (X = H, C). The populations of these silicon environments were calculated using the integrated intensities of the ^{29}Si MAS NMR spectra, and are listed in Table 2. As alkoxysilane grafting takes place on the silica surface there is a decrease on the Q^2 and Q^3 peak areas, and an increase in the Q^4, which proves that there has been a conversion from Si–OH to fully condensed Si-O-Si species. This fact, together with the presence of T^1 [R–Si(OSi)(OX)$_2$], T^2 [R–Si(OSi)$_2$(OX)] and T^3 [R–Si(OSi)$_3$] functionalities in the CP spectra at around −48, −57 and −66 ppm, respectively, explicitly confirms the existence of covalent linkages between the silica surface and the organic groups in **MSNs-COOH$_{ext}$** and **MSNs-G3** materials. The weak relative intensity of the signals for the *T* groups in the CP measurement for **MSNs-G3** material is due to the low proportion of this silicon environment in the silylated **G3** dendron.

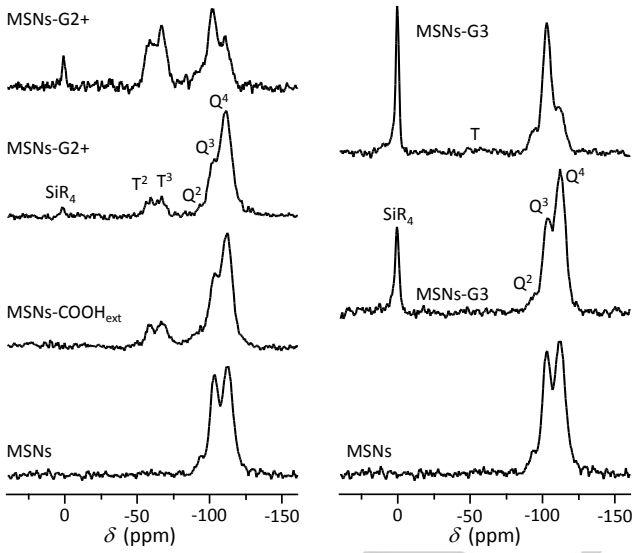

Figure 4. ^{29}Si MAS NMR spectra of **MSNs-G2+** (left) and **MSNs-G3** (right) materials (R = methyl and methylene groups of the dendrons framework). Spectra at the top of the figure correspond with the ^{29}Si CP MAS NMR measurements.

Remarkably, broad signals centred at *ca.* 1 ppm in the **MSNs-G2+** and **MSNs-G3** spectra are attributed to the silicon atoms of the framework of the dendrons, since these chemical shifts are very similar to those measured for the corresponding dendrons. Taking into account the different number of these silicon atoms in each dendron structure, the *SiR$_4$/Q* ratio for the **MSNs-G2+** material derived from its spectrum is 0.005, suggesting a small amount of **G2+** dendron in this material. The *SiR$_4$/Q* ratio of the **MSNs-G3** material increases almost five times, to 0.024. These results are in agreement with previous TG and AQE data, revealing that the straight functionalization route with a neutral dendron is a best option to achieve a higher degree of carbosilane dendron anchorage, versus the two steps route with a cationic dendron. Even **G2+** is a smaller dendron generation, electrostatic repulsions indeed outweigh steric hindrance in a neutral higher generation.

Table 2. Peak areas (%) of the silicon Q^n units on the basis of deconvolution of ^{29}Si MAS NMR spectra of MSNs materials.

Material	peak area (%)						
	Q^2	Q^3	Q^4	$(Q^2 + Q^3)/Q^4$ [a]	SiR_4 [b]	Q^n	$(SiR_4)/Q$ [c]
MSNs	6.7	40.2	53.1	0.88	---	100	0
MSNs-COOH$_{ext}$	3.6	26.7	69.7	0.43	---	100	0
MSNs-G2+	3.0	26.0	71.0	0.41	1.5	98.5	0.005
MSNs-G3	5.0	32.9	62.1	0.61	14.2	85.8	0.024

[a] Relative ratio of partially to fully condensed silicon sites. [b] Integrated intensity of the whole *SiR$_4$* peak area. [b] *SiR$_4$* to *Q* units ratio calculated taking into account that **G2+** dendron possesses 3 *SiR$_4$* units and **G3** dendron possesses 7 *SiR$_4$* units.

As expected, the populations of silicon Q^n environments in **MSNs-COOH$_{ext}$** and **MSNs-G2+** materials is practically the same. In fact, this data reflect no change, since the alkoxysilane grafting over the silica surface takes place in the first reaction step. The decrease in Q^2 and Q^3 sites is quite pronounced for **MSNs-COOH$_{ext}$** sample, although Q^2 sites are still present. Moreover, the relative ratio of partially to fully condensed silicon sites, $(Q^2 + Q^3)/Q^4$, confirms that the inner surface of the channels were preserved from functionalization, since this step were performed before the surfactant extraction stage.

The decrease in Q^2 and Q^3 populations, or decrease in $(Q^2 + Q^3)/Q^4$ ratio, is produced in a lower extent for **MSNs-G3** sample due to steric hindrance between third generation dendrons that leads to a lower coverage of the silica surface. In fact, the obtained values for **MSNs-G3** also suggest that the bulky **G3** dendrons were mainly grafted onto the external surface of the MSNs. These findings are also verified with the N_2 sorption studies detailed below. Hence, Si–OH groups would be kept unreacted due to steric interference effect which affects not only to the surface coverage but also to the inner functionalization of the mesoporous channels.

The mesostructure of the materials before and after organic functionalization was examined by powder X-ray diffraction (Figure 5). The starting MSNs material gave a well resolved XRD pattern with three characteristic reflection peaks *(10)*, *(11)* and *(20)*, indexed to a highly ordered *p6mm* mesoporous symmetry. All the materials exhibited the hexagonal mesostructure with the more intense characteristic *(10)* reflection clearly observed between 2.22 and 2.33 degrees (2θ), therefore, the lattice spacing of the MSNs materials remains virtually unaffected after carboxylic acid and dendron functionalization, with mean values of around 3.9 nm for all

materials (see inset table of Figure 5). The high ordered *(11)* and *(20)* reflections were clearly observed in the organically functionalized **MSNs-COOH$_{ext}$**, but only one strong diffraction maximum, the *(10)* reflection, was detected in the XRD patterns of **MSNs-G2+** and **MSNs-G3** samples. To further confirm whether this fact is just due to distortion of the measurement because of the high organic content, diffractograms were also collected from dendron functionalized samples subjected to a calcination process, being observed that the X-ray diffraction pattern is recovered. Nonetheless, TEM investigations confirmed the existence of typical hexagonal mesostructure in dendron functionalized materials (see inset of Figure 5 for **MSNs-G3** and Figure S12).

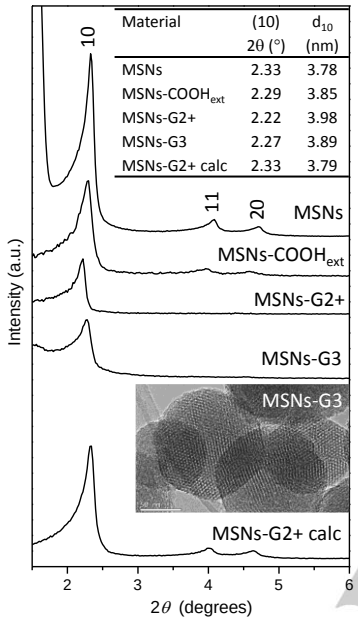

Figure 5. Small angle powder X-ray diffraction patterns of the mesoporous materials synthesized in this work. Inset table collects the scattering angles for the *(10)* XRD Bragg diffraction maximum of a 2D-hexagonal (*p6mm*) plane array of pores and their corresponding d_{10} spacing. Inset TEM image correspond to **MSNs-G3** material.

The physical properties of these mesoporous silica nanoparticles were analyzed by N_2 adsorption-desorption measurements (Figure 6 and Table 3). The surfactant extracted materials, **MSNs-COOH$_{ext}$** and **MSNs**, exhibit characteristic type IV BET isotherms with no observed hysteresis loop, confirming the presence of a cylindrical, one-dimensional channel-like mesoporous structure in the nanoparticles. The N_2 isotherms present a sharp inflection at a relative pressure of 0.20-0.30 and 0.25-0.35 respectively, which corresponds to the phenomena of capillary condensation and evaporation within channel-type uniform mesopores. In addition, a secondary step at a pressure above 0.90 P/P_0 is observed, attributed to condensation in textural porosity, *i.e.*, in the macropores formed among nanoparticles after drying.

Data obtained for the materials involved in the two-step functionalization route of MSNs with cationic **G2+** dendron are showed in Figure 6.A. As expected, while **MSNs-CTAB** displays a characteristic isotherm of a nonporous material, and has a very small surface area (60 m^2g^{-1}) and negligible pore volume (0.09402 cm^3g^{-1}), after removal of the surfactant templates the extracted **MSNs-COOH$_{ext}$** possess high surface area (847 m^2g^{-1}) and large pore volume (0.66577 cm^3g^{-1}), with a pore size distribution around 2.4 nm. This value is within the typical range in MCM-41 nanoparticles, proving that organic groups were placed at the external surface of MSNs. After the cationic **G2+** dendron is covalently linked onto the nanoparticles, the surface area is reduced to 518 m^2g^{-1}, as well as the pore volume to 0.36484 cm^3g^{-1}. However, the pore diameter decreases just slightly, from 2.4 to 2.1 nm. Therefore, these facts indicate that the **G2+** dendrons are placed at the external surface of MSNs, partially blocking the pore entrances. Although the organic content associated to the **G2+** dendron is low, the intrinsic electrostatic intradendron repulsion may be forcing an outspread conformation, resembling an umbrella shape.

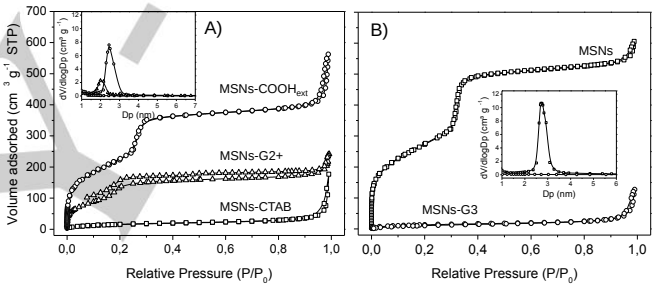

Figure 6. N_2 adsorption isotherms of MSNs materials, before and after functionalization with A) carboxylic acid groups and cationic dendron **$H_3N^+G_2(N^+Me_3)_4$** (**8**) and B) dendron **$(EtO)_3SiG_3(NMe_2)_8$** (**10**). Insets: pore size distributions for the same mesoporous samples.

Table 3. Textural parameters of MSNs materials obtained by N_2 adsorption measurements.

Material	S_{BET} (m^2g^{-1})	D_P (nm)	V_t (cm^3g^{-1})
MSNs-CTAB	59.9	-----	0.09402
MSNs-COOH	847.0	2.43	0.66577
MSNs-G2+	518.4	2.06	0.36484
MSNs	997.1	2.71	0.93646
MSNs-G3	49.5	-----	0.09185

S_{BET}: specific surface area obtained using the BET equation. D_P: pore diameter calculated using BJH method. V_t: total pore volume obtained at P/P_0 = 0.99.

Figure 6.B shows N_2 physisorption measurement of materials for the straight functionalization route of MSNs with **G3** dendron. The surface area for the bare surfactant extracted material is 997 m^2g^{-1} and the pore volume 0.93646 cm^3g^{-1}. The BJH analysis indicates a narrow pore size distribution with an

average pore diameter of 2.7 nm. The change of sorption type for the isotherm of the functionalized material **MSNs-G3**, characteristic of a nonporous material, as well as the drastic decrease in the surface area and pore volume and the BJH analysis of **MSNs-G3**, reveals that, after modification with dendron **G3**, the mesopores are almost inaccessible to nitrogen gas. This effect may be related to the drying treatment before measurement, during which the dendron shell would closely shrink onto the surface, causing the entrances of the channels to be blocked, and hence the surface area and pore volume would decrease to negligible values (Table 3). Since the third generation of these carbosilane dendrons is relatively large and the analysis of *Q* groups in the ^{29}Si MAS NMR indicates a large quantity of Si-OH groups still present in the functionalized sample, it seems rather unlikely that the anchorage takes place on the internal surface of the mesopores. Thus, is reasonable to presume that, after drying, the dendron tightly congregates on the surface of the material, thus preventing penetration of nitrogen.[42,43] Therefore, the functionalized **MSNs-G3** inherits the mesoporous structure of MSNs, and since the dendrons are not stiff and static entities, the material would still preserve the potential to act as a drug carrier by using the void mesopores.

Changes in the zeta-potential (ζ) values of the MSNs after functionalization were used to evaluate the presence of the different functional groups over the nanoparticle silica surface. As shown in Table 4, the grafting of the TESPSA alkoxysilane produced a more negative ζ-potential value compared to the bare MSNs, due to the coexistence of negative charged -SiO^- groups of silica in water plus -COO^- groups from the new carboxylic acid functionalities. The subsequent introduction on **MSN-COOH$_{ext}$** of **G2+** dendron, which contains four intrinsic ammonium moieties per molecule, balances to some extent the negative charges, thus resulting in a moderate positive ζ-potential value of 10.3 mV. Nonetheless, a drastic change from negative to positive ζ-potential value is observed when **G3** dendron is anchored onto the MSNs external surface, from −27.1 mV for bare MSNs to +35.0 mV. This result is consistent with a positive charged surface due to an acid-base equilibrium of protonation of the tertiary amine groups, as well observed on NMR experiments. The positive charges in the external surface of both materials are expected to allow adsorption of negatively charged nucleic acid fragments, being responsible of the DNA complexation by the materials.

Table 4. ζ-potential values and hydrodynamic particle size in water medium of MSNs materials.

Material	ζ-potential (mV)	Hydrodynamic size (nm) [a]
MSNs	−27.1 ± 0.6	122 ± 30
MSNs-COOH$_{ext}$	−35.2 ± 1.0	190 ± 35
MSNs-G2+	+10.3 ± 0.4	531 ± 100
MSNs-G3	+35.0 ± 1.1	142 ± 38

[a] Maximum of the size distribution, measured by DLS.

The particle diameter of each batch of particles was determined by dynamic light scattering (Table 4) showing a size distribution usually comprised between 120-190 nm and pointing out that the nanoparticle size is not significantly altered during the dendron grafting process. Only in the case of **MSNs-G2+**, the resulting particles exhibit a higher size distribution, up to 500 nm, but this value can be explained due to aggregation of particles in the conditions of the DLS measurement, as a consequence of their barely positive surface charge at this situation, +10 mV, which is far from the colloidal stability zone.[44]

Oligo ssDNA^{Cy3} adsorption into MSNs and dendron functionalized MSNs materials

The nucleic acid binding capacity of the dendron functionalized materials was determined using a fluorescence spectroscopy assay using as DNA probe a short single stranded DNA sequence (21 nucleotides) tagged with the fluorophore cyanine dye Cy3 (ssDNA^{Cy3}). A solution of ssDNA^{Cy3} was incubated with increasing amounts of the dendron functionalized MSNs materials, so the nucleic acid to nanoparticle ratio, expressed as P/N molar ratio, ranged from 1/0 to 1/20. The fluorescence measurements of the initial solution and the supernatant were compared to determine by difference the amount of ssDNA^{Cy3} that was loaded into the MSNs materials (Figure 7.A). The higher DNA binding capacity was found for **MSNs-G3** material, since it is able to bind all available DNA molecules from a P/N ratio of 1/10. However, the **MSNs-G2+** material still has not capture the total amount of DNA at a P/N ratio of 1/20. In addition, the same P/N molar ratio signifies a DNA to MSNs mass ratio different for both dendron functionalized materials, representing a very high material concentration needed in the case of **MSNs-G2+**. For example, the P/N molar ratio 1/10 represents a mass ratio for DNA/MSNs-G3 of 1/26 and for DNA/MSNs-G2+ of 1/75, which is three times more. Therefore, only **MSNs-G3** material was considered to be evaluated as vector for ssDNA cell uptake. The oligo DNA adsorption capacity of **MSNs-G3** and the unmodified MSNs represented as a function of material concentration is shown in Figure 7.B. As expected, due to the isoelectric point of silica (*ca.* 2.0), the bare MSNs present an ineffective DNA binding. The negatively charged MSNs surface in PBS is unable to electrostatically bind also negatively charged DNA fragments.

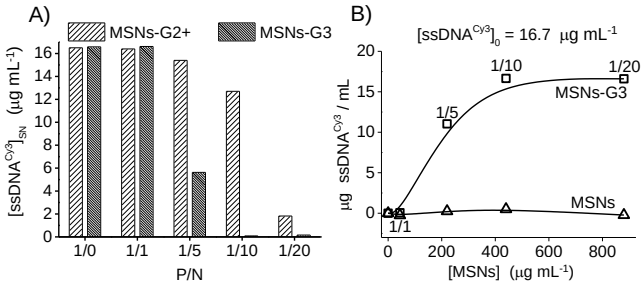

Figure 7. A) ssDNA^{Cy3} concentration on the supernatant after incubation of the initial ssDNA^{Cy3} solution with increasing amounts of the different dendron functionalized MSNs. B) Adsorption of ssDNA^{Cy3} as a function of nanoparticle concentration for bare MSNs and **MSNs-G3** materials. The colour version of this figure is available in the Supporting Information for this article.

After the adsorption of ssDNA^{Cy3}, **MSNs-G3** material was investigated with High Resolution Scanning Electron Microscopy (HR SEM) in gentle beam mode, in which case the sample does not need a previous coating with a conductive film. As can be seen in Figures 8 and S13, the load with the nucleic acid does not alter the morphology of the nanoparticles neither produces their agglomeration. In addition, the organic coverage of the nanoparticles, **G3** dendron and ssDNA^{Cy3}, is homogeneously wrapping the nanoparticles surface, as can be observed in the TEM micrograph of the negative stained sample (Figure 8, right).

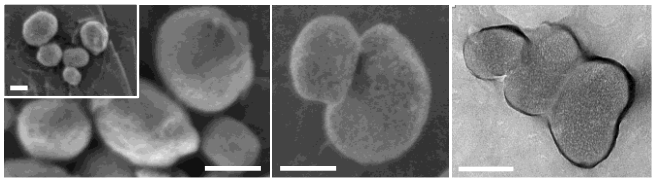

Figure 8. Images of **MSNs-G3** after ssDNA^{Cy3} adsorption (P/N molar ratio 1/10), scale bar is 100 nm. HR SEM micrographs of the untreated sample, *i.e.* without conductive coating, were taken in Gentle-Beam mode at 0.50 kV (left and centre). TEM micrograph (right) was performed on a sample treated with PTA for negative staining of organic matter.

In vitro cell studies

Cell uptake of dendron functionalized **MSNs-G3** was investigated at different concentrations or doses in comparison with the bare material MSNs. The degree of internalization was determined by flow cytometry quantifying the living cells that exhibited green fluorescence. As shown in Figure 9.A, unfunctionalized MSNs are scarcely taken up by the cells after 2 h of contact time, not existing significant differences with respect to the control ($p > 0.05$). With the higher dose (MSNs 10 μgmL^{-1}) just a 10% is achieved and virtually no particles remain internalized at 24 and 48 h. A possible aggregation effect in cell culture medium of the bare MSNs may take place and, moreover, the uptake of nonfunctionalized negatively charged silica nanoparticles is not a favourable process taking into account that the resting potential of cell membranes is usually negative. Although efficient uptake has been shown for MSNs at the same concentration but smaller size, in such case the smaller size may lead to an enhanced nonspecific cellular uptake.[45,46]

Nevertheless, dendron functionalized **MSNs-G3** are initially internalized up to values of 40% and 65% for doses 5 and 10 μgmL^{-1} respectively, existing important significant differences ($p < 0.005$) compared to the control and MSNs samples, and this results are consistent with electrostatic interaction. The dendritic wedges give a positive charge density onto the nanoparticles surface which produces a greater stabilization and dispersion in cell culture medium as well as the absence of electrostatic repulsion with cell membranes and, consequently, an improvement in the process of cellular internalization. Moreover, carbosilane dendritic frameworks which are hydrophobic are expected to better interact with cell membranes what might improve transfection efficiency, as well as facilitate the crossing of the blood brain barrier.[47]

The internalization percentages increase to a maximum value during the first 24 h. Since after the 2 first hours of contact time the medium is removed and replaced with free-MSNs medium, this effect is due to cells that continue gradually incorporating the **MSNs-G3** nanoparticles which remain adsorbed to the membrane. The reduction in the percentage of internalization at 48 h can be attributed to two factors. On the one hand there is also a process of exocytosis[48] and, on the other hand, it must be taken into account that the cellular proliferation means a greater number of cells and therefore a dissemination of the nanoparticles initially internalized. At all times the **MNS-G3** cell uptake is dose-dependent reaching a maximum value of 84% in the first stage (2-24 h) for the higher dose.

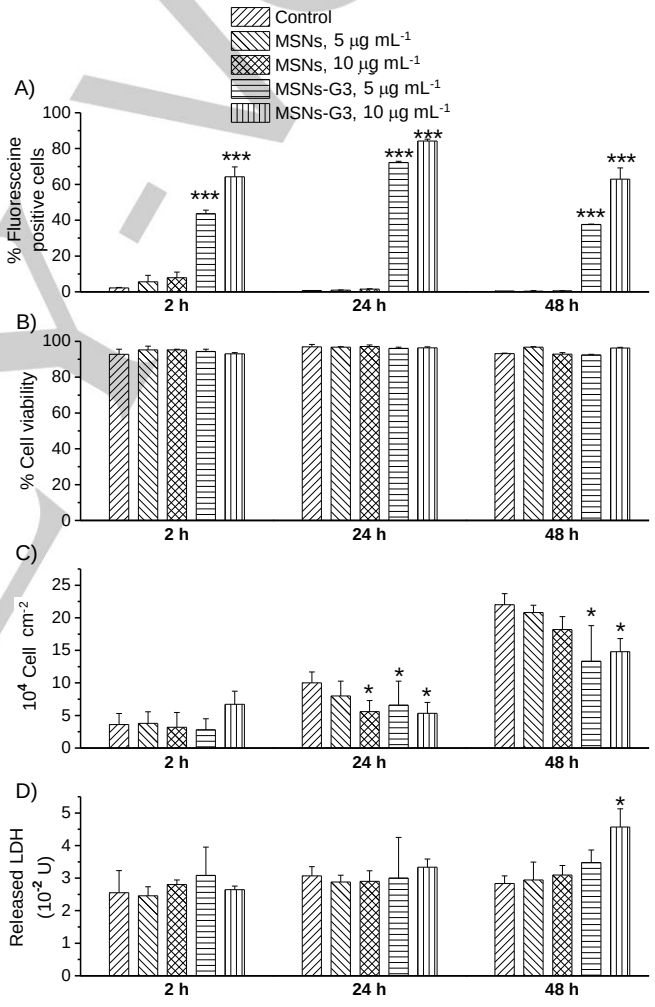

Figure 9. Cell uptake and cytotoxicity studies of bare MSNs and dendron functionalized **MSNs-G3** at different doses evaluated on HOS cells at different times. A) Per cent of HOS cells with internalized nanoparticles measured by flow cytometry. Statistical significance: ***$p < 0.005$. B) Cell viability evaluated by propidium iodide negative fluorescent. No significant differences with respect to the control. C) Cell population. Statistical significance: *$p < 0.05$. D) LDH released to medium culture. Statistical significance: *$p < 0.05$. The colour version of this figure is available in the Supporting Information for this article.

None of the studied materials (bare MSNs and **MSNs-G3**), at the different doses (5 and 10 μgmL^{-1}) and times assayed (2, 24 and 48 h), produced significant differences in cell viability as compared to the control ($p > 0.05$) (Figure 9.B). As shown in Figure 9.C at 2 h there are not significant differences in cell proliferation of cultured HOS with the different samples with respect to the control ($p > 0.05$). At 24 and 48 h osteoblastic cell lineage slightly decreases its proliferation in the case of bare MSNs, probably due to the absence of cell uptake.

However, HOS cells cultured with **MSNs-G3** slowdown their proliferation significantly, probably due to the nanoparticle internalization process occurring in these samples ($*p < 0.05$). From the measurements of LDH released to the medium (Figure 9.D) it is explained that both the presence and low internalization of MSNs and the high internalization of **MSNs-G3** during the contact time and the first 24 h do not cause cell cytotoxicity (no significant differences with respect to the control), since the integrity of cell membranes of osteoblastic cells HOS are not affected. The internalization process of **MSNs-G3** causes a moderate cytotoxicity at 48 h for the higher dose ($*p < 0.05$).

MSNs-G3 material was also tested at a higher dose (50 μgmL^{-1}), resulting in a significant decrease of 20% in cell viability values with respect to the control ($*p < 0.05$). This effect is probably due to very high internalization levels, up to 90%, in the two hours of contact time. In addition the internalization produces a pronounced deceleration in the cell proliferation at 24 and 48 h ($***p < 0.005$) and high levels of LDH released to the medium at 48 h compared to the control ($***p < 0.005$), indicating cytotoxicity due to cell membrane fragmentation (Figure S14).

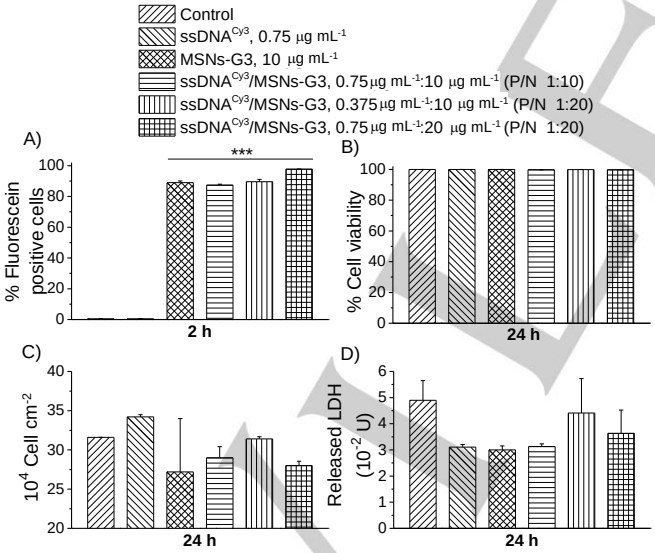

Figure 10. Cell uptake and cytotoxicity studies of dendron functionalized **MSNs-G3** and ssDNA^{Cy3} oligonucleotide at different doses evaluated on HOS cells. A) Per cent of HOS cells with internalized nanoparticles measured by flow cytometry. Statistical significance: $***p < 0.005$. B) Cell viability evaluated by propidium iodide negative fluorescent. No significant differences with respect to the control. C) Cell population. D) LDH released to medium culture. The colour version of this figure is available in the Supporting Information for this article.

Once checked on the one hand the ability of materials **MSNs-G3** to adsorb ssDNA and moreover its internalization capacity in HOS cells without affecting their viability, a trial was conducted to verify their possible use as vectors of genetic material. The ssDNA^{Cy3}, which contains a traceable fluorophore that allows the visualization of nucleic acid loaded onto the nanoparticles and its internalization process, was used as a DNA probe. Cells were incubated with two different doses of **MSNs-G3** with DNA loaded onto the nanoparticles at two different P/N, 1:10 and 1:20. As additional references to the control, free oligo and nanoparticles were also incubated with the cells under same conditions. As expected, there are high levels of cell uptake (Figure 10.A) of **MSN-G3** nanoparticles at different concentrations of probe and nanoparticles. Due to the high internalization of nanoparticles, cells were maintained in culture for 24 h to assess differences in viability, proliferation and cytotoxicity. The cell viability (Figure 10.B) is maintained at values greater than 95%, therefore representing a good viability of the cells after nanoparticle internalization. In addition the values of cell proliferation are concordant with the LDH released to the culture medium (Figures 10.C and 10.D) without significant differences with the control and confirming the absence of cellular cytotoxicity after the entry of the vector with the DNA probe.

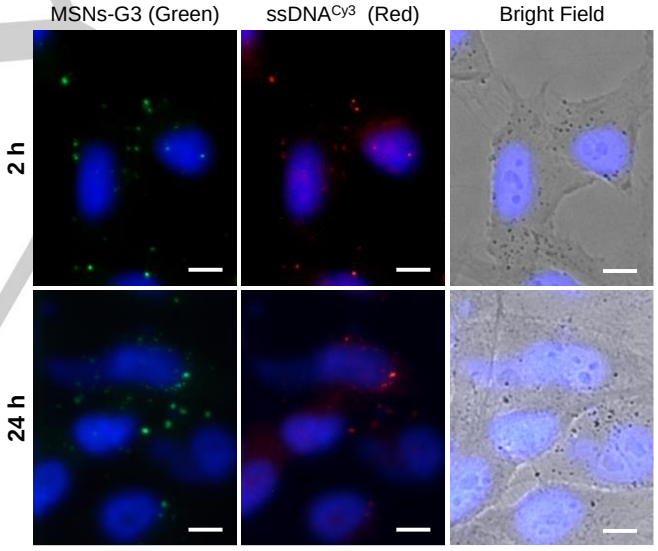

Figure 11. Fluorescence microscopy images at 2 and 24 h of HOS cell culture after incubation with ssDNA^{Cy3}/MSNs-G3 (0.75 μgmL^{-1} : 10 μgmL^{-1}) (P/N molar ratio 1:10). Cell nucleus was stained with DAPI and blue field overlays in all images. The first column corresponds to fluorescein green fluorescence from nanoparticles. The second column corresponds to the Cy3 red fluorescence from the ssDNA. The third line corresponds to the bright field image of the same regions. Scale bar is 10 μm. The colour version of this figure is available in the Supporting Information for this article.

In addition to the quantification by FACS analysis, the same experiment was qualitative analyzed by fluorescence microscopy (Figure 11). **MSNs-G3** material, labelled with fluorescein, is detected in the green field as discrete dots, which indicates nanoparticle aggregation. It can be found that after 2 h

of contact time HOS cells have internalized the **MSNs-G3** though some nanoparticles remain attached to the cell membrane. After 24 h the green fluorescence can be seen in cytoplasm and around the nucleus. After 24 h, as well as after 2 h, internalized **MSNs-G3** also emits red fluorescence in the red field. Since no Cy3 signal was found in the untreated cells or in those cells treated with free oligo-Cy3 (data not shown), the uptake of ssDNA^{Cy3} have been produced via the **MSNs-G3** material acting as vector. Consequently carbosilane dendron functionalized **MSNs-G3** exhibited a strong ability to transport oligo DNA (a model for siRNA) to HOS cells.

Conclusions

A novel carbosilane dendron-functionalized mesoporous silica nanocarrier able to transport oligonucleotide single strands within tumoral cells has been presented. As a first stage, the preparation of a new nonviral vector based on mesoporous silica nanoparticles functionalized with carbosilane dendrons has been investigated. Two different carbosilane dendrons, with cationic and neutral amine terminal groups, were used and, therefore, two different synthetic approaches for their covalent anchorage to the external silica surface were assayed. The synthetic approaches were a two-step route for the grafting of the second generation of a cationic dendron (**G2+**) and a straight route for the grafting of the third generation of a neutral dendron (**G3**). The results indicated a higher level of dendron functionalization for the neutral G3 dendron. Hence, electrostatic repulsion when **G2+** was attached played an important role, exceeding the expected steric hindrance for **G3** dendron.

These new hybrid materials have been precisely characterized and their properties as potential gene delivery nanocarriers have been tested *in vitro*, showing a significant higher DNA adsorption efficacy for the **MSNs-G3** material. In addition, this vector shows high levels of internalization in a HOS cell line, presenting low cytotoxicity. The cell uptake of **MSNs-G3** material is dose dependent and optimum doses have been determined ensuring the biocompatibility of this nonviral vector. With the assayed doses an internalization level of *ca.* 84% is achieved in a short time, during the first 2-24 h. More importantly, after the internalization process the cells keep intact the integrity of their plasmatic membrane, confirming the absence of cytotoxicity for the assayed doses.

Furthermore, the existence of a highly ordered pore network inside the silica matrix can be used to house other type of molecules which would enhance its gene delivery properties or transform this material into a multidrug delivery device for a combined drug/gene therapy. Further work is on-going in this line, aiming at explore the suitability of this hybrid nanosystem in clinical applications for HIV and cancer treatment, as well as to test its targeting capacity and *in vivo* response.

Experimental Section

Reagents

All reactions for the synthesis of dendrons and for the chemical modification of the silica surface were performed under an inert atmosphere using standard Schlenk techniques. Tetrahydrofurane and dichloromethane were dried by standard procedures and distilled immediately prior to use.

Compounds **PhtG_n(NMe_2HCl)$_m$** and **H_2NG_n(NMe_2)$_m$** were synthesized as published.[30] Fluorescein isothiocyanate (FITC), tetraethylorthosilicate (TEOS), cetyltrimethylammonium bromide (CTAB), *N*-(3-Dimethylaminopropyl)-*N'*-ethylcarbodiimide hydrochloride (EDC.HCl) and iodomethane (MeI) were purchased from Sigma-Aldrich. A single DNA strand, 21 nucleotides long and tagged with a fluorescent moiety (Cy3 labeled oligonucleotide, 1 µmol synthesis scale, reverse phase purification, [Cy3]TTATCGCTGATTCAAGACTGA 5'-3' sequence) was also purchased from Sigma-Aldrich. 3-Aminopropyltriethoxysilane (APTS), 3-isocyanatopropyltriethoxysilane and 3-(triethoxysilyl)propylsuccinic anhydride (TESPSA) were purchased from ABCR GmbH & Co. KG. These compounds were used without further purification.

Deionized water was further purified by passage through a Milli-Q Advantage A-10 Purification System (Millipore Corporation) to a final resistivity of 18 MΩ cm or above. All other chemicals (HCl 37% wt., HI 57% wt., Na_2CO_3, absolute EtOH, dry toluene, NaOH, etc.) were of the highest quality commercially available and used as received.

Synthesis of PhtG_n(NMe_2)$_m$ (1, 2, 3)

PhtG_1(NMe_2)$_2$ (1). This dendron was prepared from the corresponding hydrochloride product PhtG_1(NMe_2HCl)$_2$ (0.421 g, 0.72 mmol) dissolved in H_2O/$CHCl_3$ (1:1, 20 ml). To this mixture a Na_2CO_3 solution was added drop by drop (0.153 g, 1.44 mmol) and this final mixture was stirred for 15 minutes at room temperature. Finally the aqueous phase was removed and the organic phase was dried in vacuo to get **1** as a pale yellow oil (0.342 g, 93 %).

PhtG_2(NMe_2)$_4$ (2). This dendron was prepared from PhtG_2(NMe_2HCl)$_4$ (0.472 g, 0.43 mmol) and Na_2CO_3 (0.183 g, 1.73 mmol) using the preparative procedure for **1**, to get PhtG_3(NMe_2)$_8$ as a pale yellow oil (0.395 g, 96 %).

PhtG_3(NMe_2)$_8$ (3). This dendron was prepared from PhtG_3(NMe_2HCl)$_8$ (0.527 g, 0.25 mmol) and Na_2CO_3 (0.212 g, 2.00 mmol) using the preparative procedure for **1**, to get PhtG_3(NMe_2)$_8$ as a pale yellow oil (0.380 g, 84 %).

Synthesis of PhtG_n(N^+Me_3)$_m$ (4, 5, 6)

PhtG_1(NMe_3I)$_2$ (4). To a diethyl ether (20 ml) solution of **1** (0.342 g, 0.67 mmol) were added 0.10 ml of a MeI solution (1.61 mmol). The resulting solution was stirred for 16 h at room temperature and then evaporated under reduced pressure and washed twice with hexane (20 ml). **4** is got after drying as a white solid (0.532 g, 81 %).

PhtG_2(NMe_3I)$_4$ (5). 5 was prepared using a similar method to that described for **4**, starting from **2** (0.395 g, 0.42 mmol) and MeI (0.12 ml, 1.92 mmol) to get PhtG_3(NMe_3I)$_8$ as a white solid (0.506 g, 80 %).

$PhtG_3(NMe_3I)_8$ (6). **6** was prepared using a similar method to that described for **4**, starting from **3** (0.380 g, 0.21 mmol) and MeI (0.12 ml, 1.92 mmol) to get **6** as a white solid (0.611 g, 99 %).

Synthesis of $H_3N^+G_n(N^+Me_3)_m$ (7, 8 or G2+, 9)

$NH_3IG_1(NMe_3I)_2$ (7). To a MeOH:water solution (20:1) of 4 (0.532 g, 0.67 mmol), an excess of hydrazine was added (0.05 ml, 1.67 mmol) and the reaction mixture was stirred at 80 °C in a sealed ampoule for 16 hours. After this period of time the solution was evaporated and the residue was solved in water, then 0.18 ml of a HI solution (1.34 mmol) were added under argon atmosphere. After 20 minutes, the reaction mixture was filtered and the aqueous phase was evaporated. The residue was washed twice with diethyl ether and finally dried to give $NH_3IG_2(NMe_3I)_4$ as a white solid (0.324 g, 61 %).

$NH_3IG_2(NMe_3I)_4$ (8, G2+). 8 was prepared using a similar method to that described for 7, starting from 5 (0.506 g, 0.33 mmol), N_2H_4 (0.02 ml, 0.82 mmol) and HI (0.11 ml, 0.84 mmol) to get $NH_3IG_3(NMe_3I)_8$ as a white solid (0.343 g, 68 %).

Data for 8: ^{1}H NMR (500 MHz, [D$_6$]DMSO, 25 ºC): δ = -0.07 (s, 3 H; Si*Me*), 0.04 (s, 6 H; Si*Me*), 0.57 (m, 10 H; Si*CH*$_2$CH$_2$C*H*$_2$Si and NCH$_2$CH$_2$CH$_2$C*H*$_2$Si), 0.86 (t, J_a = 8.2 Hz, 8 H; Si*CH*$_2$CH$_2$S), 1.29 (m, 6 H; SiCH$_2$C*H*$_2$CH$_2$Si and NCH$_2$CH$_2$C*H*$_2$CH$_2$Si), 1.52 (m, 2 H; NCH$_2$C*H*$_2$CH$_2$CH$_2$Si), 2.64 (t, J_a = 8.4 Hz, 8 H; SiCH$_2$C*H*$_2$S), 2.78 (m, 2 H; NC*H*$_2$), 2.90 (t, J_b = 8.2 Hz, 8 H; SC*H*$_2$CH$_2$NMe$_3^+$), 3.10 (s, 36 H; SCH$_2$CH$_2$N*Me*$_3$I), 3.54 (t, J_b = 8.3 Hz, 8 H; SCH$_2$C*H*$_2$NMe$_3^+$), 7.62 ppm (bs, 3 H; -N*H*$_3^+$). ^{13}C NMR (62.9 MHz, [D$_6$]DMSO, 25 ºC): δ = -5.6 (Si*Me*), 12.7 (NCH$_2$CH$_2$CH$_2$*C*H$_2$Si), 13.6 (Si*C*H$_2$CH$_2$S), 17.2, 17.4 and 17.5 (Si*C*H$_2$*C*H$_2$*C*H$_2$Si), 20.0 (NCH$_2$CH$_2$*C*H$_2$CH$_2$Si), 23.1 (S*C*H$_2$CH$_2$NMe$_3^+$), 26.4 (SiCH$_2$*C*H$_2$S), 30.4 (NCH$_2$*C*H$_2$CH$_2$CH$_2$Si), 38.4 (N*C*H$_2$), 51.7 (SiCH$_2$CH$_2$N*Me*$_3^+$), 63.9 ppm (SCH$_2$*C*H$_2$NMe$_3^+$). ^{15}N NMR: δ = -329.5 (*N*Me$_3^+$), -346.3 ppm (*N*CH$_2$). ^{29}Si NMR (99.4 MHz, [D$_6$]DMSO, 25 ºC): δ = 2.5 ppm (G$_2$–*Si*Me). Elemental analysis calcd (%) for $C_{41}H_{100}I_5N_5S_4Si_3$ (1510.30 gmol^{-1}): C 32.61, H 6.67, N 4.64, S 8.49; found: C 32.55, H 6.65, N 4.40, S 8.18.

$NH_3IG_3(NMe_3I)_8$ (9). 9 was prepared using a similar method to that described for 7, starting from 6 (0.380 g, 0.21 mmol), N_2H_4 (0.02 ml, 0.52 mmol) and HI (0.12 ml, 0.92 mmol) to get $NH_3IG_3(NMe_3I)_8$ as a white solid (0.611 g, 99 %).

Synthesis of carbosilane dendron $(EtO)_3SiG_3(NMe_2)_8$ (10 or G3)

$(EtO)_3SiG_3(NMe_2)_8$ (10). Under inert atmosphere, a solution of 3-isocyanatopropyltriethoxysilane (20 μL, 7.6 × 10^{-5} mol, 1 eq) in dry CH_2Cl_2 (10 mL) was added dropwise to a stirred solution of **$H_2NG_3(NMe_2)_8$** (0.128 g, 7.7 × 10^{-5} mol, 1 eq) in dry CH_2Cl_2 (10 mL). The reaction mixture was stirred overnight at room temperature and then filtered off. After solvent removal, the filtrate appeared as a light-brownish oil in quantitative yield, which was kept under inert atmosphere.

Data for 10: ^{1}H NMR (500 MHz, $CDCl_3$, 25 ºC): δ = -0.12 (s, 9 H; Si*Me*), -0.02 (s, 12 H; Si*Me*), 0.45 (m, 2 H; (EtO)$_3$SiC*H*$_2$), 0.50 (m, 16 H; Si*C*H$_2$CH$_2$C*H*$_2$Si), 0.58 (m, 8 H; SiCH$_2$CH$_2$C*H*$_2$Si), 0.63 (m, 2 H; NCH$_2$CH$_2$CH$_2$C*H*$_2$Si), 0.86 (t, 16 H; Si*CH*$_2$CH$_2$S), 1.17 (t, 9 H; (C*H*$_3$CH$_2$O)$_3$Si), 1.25 (m, 14 H; SiCH$_2$C*H*$_2$CH$_2$Si + NCH$_2$CH$_2$C*H*$_2$CH$_2$Si), 1.47 (m, 2 H; (EtO)$_3$SiCH$_2$C*H*$_2$CH$_2$), 1.56 (m, 2 H; NCH$_2$C*H*$_2$CH$_2$CH$_2$Si), 2.23 (s, 48 H; SCH$_2$CH$_2$N*Me*$_2$), 2.47 (m, 16 H; SCH$_2$C*H*$_2$NMe$_2$), 2.52 (m, 16 H; SiCH$_2$C*H*$_2$S), 2.60 (m, 16 H; SC*H*$_2$CH$_2$NMe$_2$), 3.10 (m, 4 H; NC*H*$_2$), 3.77 (q, 6 H; (CH$_3$C*H*$_2$O)$_3$Si), 4.50 (m, 1H; NHCON*H*), 4.64 ppm (m, 1H; N*H*CONH). ^{13}C{^{1}H} NMR (62.9 MHz, $CDCl_3$, 25 ºC): δ = -5.0 (Si*Me*), -4.8 (Si*Me*), -4.7 (Si*Me*), 7.9 ((EtO)$_3$Si*C*H$_2$), 14.1 (NCH$_2$CH$_2$CH$_2$*C*H$_2$Si), 14.9 (Si*C*H$_2$CH$_2$S), 18.57 ((*C*H$_3$CH$_2$O)$_3$Si), 18.61, 18.71, 19.12 (Si*C*H$_2$*C*H$_2$*C*H$_2$Si), 21.7 (NCH$_2$CH$_2$*C*H$_2$CH$_2$Si), 24.0 ((EtO)$_3$SiCH$_2$*C*H$_2$), 28.0 (S*C*H$_2$CH$_2$NMe$_2$), 30.0 (SiCH$_2$*C*H$_2$S), 34.7 (NCH$_2$*C*H$_2$CH$_2$CH$_2$Si), 40.7, 43.2 (*C*H$_2$NHCONHCH$_2$), 45.6 (SiCH$_2$CH$_2$N*Me*$_2$), 58.7 ((CH$_3$*C*H$_2$O)$_3$Si), 59.5 (SCH$_2$*C*H$_2$NMe$_2$), 158.6 ppm (NH*C*ONH). ^{29}Si NMR (99.4 MHz, $CDCl_3$, 25 ºC): δ = 1.94 (G$_3$–*Si*Me), 1.54 (G$_1$–*Si*Me), 0.91 (G$_2$–*Si*Me), -45.39 ppm (s, CH$_2$*Si*(OCH$_2$CH$_3$)$_3$). MALDI-TOF MS: *m/z* (%): 1931.96 (100) [*M* + H$^+$]$^+$ (theoretical 1932.2). Elemental analysis calcd (%) for $C_{87}H_{200}O_4N_{10}S_8Si_8$ (1931 gmol^{-1}): C 54.06, H 10.36, N 7.25, S 13.26; found: C 51.10, H 9.61, N 7.10, S 12.43.

MSNs materials synthesis

Under an inert N_2 atmosphere, APTS (20 μL, 0.09 mmol) was added over a stirred FITC (8 mg, 0.02 mmol) solution in EtOH (2 mL). The reaction mixture was stirred at RT for 2 h in the dark, and then 5 mL of TEOS were added. This solution was subsequently placed on a syringe dispenser to be transferred to the next reaction.

The cationic surfactant CTAB (1 g, 2.74 mmol) was dissolved in 480 mL of water with 3.75 mL of NaOH 2 M and the solution was heated to 80 °C under vigorous stirring. Then, the solution containing TEOS and the alkoxysilane modified fluorescein was slowly added at a constant rate of 0.25 mLmin^{-1}. After 2 h at 80 °C and vigorous stirring the suspension was cooled to room temperature, filtered and the particles washed by centrifuging several times with water, EtOH and finally dried.

Removal of the surfactant was carried out by ion exchange using an extracting solution of NH_4NO_3 (10 gL^{-1}) in EtOH/H_2O (95:5, v/v) in a ratio of 3 g of the as-synthesized MSNs per litre of extracting solution. The suspension was heated to 65 °C under stirring for 2 h and then the solid was thoroughly washed with EtOH. This extraction process was repeated three times and the solid dried (S_{BET} = 997 m^{2}g^{-1}).

Surface functionalization of MSNs materials

Prior to surface functionalization MSNs materials were dehydrated at 80 °C under vacuum for 5 h and subsequently redispersed, under an inert atmosphere in the corresponding dry reaction solvent, by means of ultrasound and vortex shaking for approximately 30 min, until a fine suspension was obtained.

$MSNs\text{-}COOH_{ext.}$ For the external surface functionalization of MSNs with –COOH groups, pore surfactant containing material (40.62% wt.) was employed and therefore approximately a quarter of the specific surface area of the free-surfactant material was considered to be functionalized, assuming that it resembles the external surface of the nanoparticles.

A solution of TESPSA (0.027 g, 10% exc) in 4 mL of dry toluene was added to a vigorously stirred suspension of 0.200 g of CTAB-containing MSNs (0.119 g MSNs) in 6 mL of dry toluene and the mixture was heated to 110 °C overnight. The solid was filtered, washed exhaustively with toluene and acetone and then dried under vacuum. The CTAB surfactant was removed from the material by heating the mixture of the obtained solid in 40 mL of EtOH and 1 mL of concentrated HCl overnight at 60 °C and then the solid was thoroughly washed with EtOH. This extraction process was repeated two times for 2 h and the solid dried under vacuum. The nominal or theoretical value of –COOH for this material is 1.3521 × 10^{-3} –COOH molg^{-1} SiO_2 (S_{BET} = 847.0 m^{2}g^{-1}).

MSNs-G2+. A solution of EDC.HCl (0.259 g, 10 eq per nominal –COOH group) in 3 mL of H_2O was added to a suspension of 0.100 g of MSNs-

$COOH_{ext}$ in 3 mL of H_2O. the mixture was gently stirred for 2 h at room temperature and subsequently a solution of 13 mg of $\mathbf{H_3N^+G_2(N^+Me_3)_4}$ (1 eq per 16 eq nominal –COOH group, 6.25%) in 0.5 mL of water was added. The stirring was maintained overnight at RT and then the solid filtered, exhaustively washed with water, EtOH and vacuum dried. The molar amount of G2+ dendron per gram of **MSNs-G2+** material estimated from AQE data is 3.04×10^{-5} molg^{-1}.

MSNs-G3. For the silica surface functionalization the freshly obtained solution of silyl-functionalized dendron precursor $\mathbf{(EtO)_3SiG_3(NMe_2)_8}$ was checked (FTIR and ^{1}H NMR spectroscopies) and subsequently used in the post-grafting reaction with the MSNs. Under inert atmosphere, a solution of 3-isocyanatopropyltriethoxysilane (13 μL, 5.12×10^{-5} mol, 0.8 eq) in dry CH_2Cl_2 (5 mL) was added dropwise to a stirred solution of $\mathbf{H_2NG_3(NMe_2)_8}$ (0.1079 g, 6.41×10^{-5} mol, 1 eq) in dry CH_2Cl_2 (10 mL). The reaction mixture was stirred overnight at room temperature and then filtered off to be immediately used in the next step. The solution was concentrated to *ca.* 5 mL and added dropwise to a MSNs (0.303 g) suspension in dry CH_2Cl_2. The mixture was stirred overnight, filtered, washed exhaustively with CH_2Cl_2 and CH_2Cl_2/Et_2O (1:1) and dried under vacuum. The molar amount of **G3** dendron per gram of **MSNs-G3** material estimated from AQE data is 1.43×10^{-4} molg^{-1}.

Oligo ssDNA^{Cy3} adsorption into MSNs materials

In order to determine the ssDNA^{Cy3} concentration in the solutions, a standard calibration curve of fluorescence versus concentration was first obtained using λ_{EX} = 535 nm and λ_{EM} = 570 nm, giving the equation: [ssDNA^{Cy3}] = $2035.2 \times F_{570} - 11.2$ (R^2 = 0.991). 5 μL of a stock ssDNA^{Cy3} solution (1 μgμL^{-1} in tris-EDTA buffer) were mixed with a series of increasing amounts of well dispersed aqueous suspensions of MSNs (1 mgmL^{-1}) and the final volume was completed to 300 μL in 1.5 mL eppendorf centrifuge tube. The mixture was dispersed by vortex for 30 s and incubated at 37 °C in an orbital shaker at 100 rpm for 30 min. Suspensions were separated by centrifugation at 10000 rpm for 5 min and 250 μL of the supernatant were analyzed in a fluorescence spectroscope.

Fluorescence spectroscopy was analyzed with a Microplate fluorescence reader Synergy4 (Biotech) using λ_{EX} = 535 nm and λ_{EM} = 570 nm.

Cell culture

A human osteoblast-like cell line denoted HOS was used to test the internalization, cytotoxicity and biocompatibility of the nanomaterials and their oligo DNA transfection ability. This cell line, obtained through the European Collection of Cell Cultures (ECACC, no. 87070202), was derived from an osteosarcoma of a Caucasian female. The adherent cells were maintained under a 5% CO_2 atmosphere at 37 °C in T75 flasks using Dulbecco's modified Eagle's medium (DMEM) supplemented with 10% heat-inactivated fetal bovine serum (FBS), 2 mM L-glutamine, 100 μgmL^{-1} penicillin and 100 μgmL^{-1} streptomycin all supplied by Gibco). Osteoblast-like cells were routinely subcultured, passaged every 3 days at 70-80% subconfluency and seeded at 2-4·10^{4}cellscm^{-2}.

Cell uptake assay and assessment of cytotoxicity

Well dispersed suspensions of MSNs and **MSNs-G3** nanoparticles were prepared in DMEM at 1 mgmL^{-1}. 24 h prior to the experiment, HOS were seeded on 6 well culture plates at a density of 10^5 cells/well and in 2 mL growth medium. Cells were approximately 50% confluent at the time of nanoparticles addition. For control experiments, HOS cells were incubated without nanoparticles. After 24 h of cell attachment, growth medium is replaced for medium which contains MSNs nanoparticles at different concentrations (5, 10 and 50 μgmL^{-1}) and cells were incubated for 2 h at 37 °C and 5% CO_2. After that contact time, cells were thoroughly washed with tempered phosphate buffered saline (PBS) to remove nanoparticles not attached to the membrane or internalized by the cells, and further incubated in particle free medium for 24 h and 48 h.

Subsequently, in order to evaluate the internalization of the MSNs and the material biocompatibility, the medium was aspirated and the cells were washed with PBS and harvested using 0.25% trypsin-EDTA solution. After 15 min, the reaction was stopped with culture medium and the cells were then centrifuged at 280 g for 10 min and resuspended in fresh medium for the analysis by flow cytometry. A small amount of Trypan Blue (TB 0.4%) was added at that time to quench the fluorescence of the MSNs adhered in the outside membrane of the cell, as TB cannot penetrate the membranes of living cells. The percentage of cells that had internalized nanoparticles was quantified as the fraction of fluoresceine positive cells among the counted number of live cells. Cell viability was determined by addition of propidium iodide (PI 0.05% in PBS) to stain the DNA of dead cells.

A FACSCan™ (Becton Dickinson) flow cytometer was used and data were analyzed with BD CellQuest™ software, provided in the equipment. For statistical significance, at least 10^4 events were recorded in each sample and the mean of the fluorescence emitted by these single cells was used.

A cytotoxicity assay was performed with a commercial kit provided by SPINREACT (Girona, Spain). The kit was used according the specifications of the manufacturer to evaluate damages in the cells produced by the uptake of MSNs through the released lactose dehydrogenase (LDH) to the media.

An automatic cell counter (Countess™ of Invitrogen) was used to count up the number of live/dead cell per well using an appropriate dilution with DMEM/Trypan Blue (0.4%) in 1:1 vol.

DNA internalization test

DNA/MSNs complexes were prepared as previously described at P/N molar ratios of 1/10 and 1/20 and subsequently dispersed in DMEN at 10 and 20 μgmL^{-1} of MSNs. Cell uptake and FACS analysis were also performed as formerly stated. For control experiments, HOS cells were incubated without nanoparticles as well as in the presence of ssDNA^{Cy3} (0.75 μgmL^{-1}). In order to observe the ssDNA^{Cy3} adsorbed onto the **MSNs-G3** surface, cells were examined by a fluorescence microscope. After incubation the culture medium was removed, and cells were carefully washed with PBS solution. Cells were then fixed with glutaraldehyde 4% (w/v) for 20 min at 37 °C. After rinsing with PBS, cells were incubated in PBS containing 0.5% (v/v) Triton X-100 at 4 °C for 5 min and then in PBS containing bovine serum albumin (BSA 1% w/v) for 20 min at room temperature. Cells were then washed twice with PBS, and stained with DAPI (0.1 mgmL^{-1} in PBS) in the dark at room temperature for 15 min.

Fluorescence microscopy was performed with an Evos® FL Cell Imaging System equipped with tree Led Lights Cubes (λ_{EX} (nm); λ_{EM} (nm)): DAPY (357/44; 447/60), GFP (470/22; 525/50), RFP (531/40; 593/40) from AMG (Advance Microscopy Group).

Statistics

Data are expressed as means ± standard deviations of a representative of three experiments. Every experiment was performed in quadruplicate. Statistical analysis was performed using the Statistical Package for the Social Sciences (SPSS) version 19 software. Statistical comparisons were made by analysis of variance (ANOVA). Scheffè test was used for *posthoc* evaluations of differences among groups. In all statistical evaluations, $p < 0.05$ was considered as statistically significant.

Acknowledgements

This work has been supported by the Ministerio de Economía y Competitividad (MINECO) through projects MAT2012-35556 and CSO2010-11384-E (Agening Network of Excellence) to Universidad Complutense de Madrid. As well, this work has been supported by grants from MINECO (CTQ2011-23245), UAH (CCG2013/EXP032) and CAM (Consortium NANODENDMED, ref S2011/BMD-2351) to Universidad de Alcalá. This work was also supported by grants from the Ministerio de Educación for E.F.P. CIBER-BBN is an initiative funded by the VI National R&D&i Plan 2008–2011, Iniciativa Ingenio 2010, Consolider Program, CIBER Actions are financed by the Instituto de Salud Carlos III with assistance from the European Regional Development Fund.

Keywords: carbosilane dendrons • mesoporous materials • nanoparticles • gene transfection • nonviral vectors •

[1] H. Singh, J. S. E. Moyes, M. H. Huls, L. J. N. Cooper, *Cancer Gene Ther.* **2015**, *22*, 95-100.
[2] C. Sheridan, *Nat. Biotechnol.* **2011**, *29*, 121-128.
[3] J. Park, K. Singha, S. Son, J. Kim, R. Namgung, C.-O. Yun, W. J. Kim, *Cancer Gene Ther.* **2012**, *19*, 741-748.
[4] E. Herrera-Carrillo, B. Berkhout, *Gene Ther.* **2015**, *22*, 485-495.
[5] J. Kurreck, *Angew. Chem. Int. Ed.* **2009**, *48*, 1378-1398.
[6] J. Yang, H. Liu, X. Zhang, *Biotechnol. Adv.* **2014**, *32*, 804-817.
[7] X. Guo, L. Huang, *Acc. Chem. Res.* **2012**, *45*, 971-979.
[8] V. Sokolova, M. Epple, *Angew. Chem. Int. Ed.* **2008**, *47*, 1382-1395.
[9] S. Mignani, S. El Kazzouli, M. Bousmina, J.-P. Majoral, *Prog. Polym. Sci.* **2013**, *38*, 993-1008.
[10] S. Mignani, S. El Kazzouli, M. Bousmina, J.-P. Majoral, *Adv. Drug Deliv. Rev.* **2013**, *65*, 1316-1330.
[11] J. Li, A.-M. Lepadatu, Y. Zhu, M. Ciobanu, Y. Wang, S. C. Asaftei, D. Oupický, *Bioconjugate Chem.* **2014**, *25*, 907-917.
[12] A. J. Perisé-Barrios, J. L. Jiménez, Á. Domínguez-Soto, F. J. de la Mata, Á. L. Corbí, R. Gómez, M. Á. Muñoz-Fernandez, *J. Control. Release* **2014**, *184*, 51-57.
[13] K. Sarkar, P. P. Kundu, *Carbohydrate Polymers* **2013**, *98*, 495-504.
[14] P. Schilrreff, C. Mundiña-Weilenmann, E. L. Romero, M. J. Morilla, *Int. J. Nanomedicine* **2012**, *7*, 4121-4133.
[15] M. Tonga, G. Y. Tonga, G. Seber, O. Gok, A. Sanyal, *J. Polym. Sci. Part A: Polymer Chemistry* **2013**, *51*, 5029-5037.
[16] B. Huang, D. A. Tomalia, *J. Luminescence* **2005**, *111*, 215-223.
[17] S.-H. Hwang, C. N. Moorefield, P. Wang, K.-U. Jeong, S. Z. D. Cheng, K. K. Kotta, G. R. Newkome, *J. Am. Chem. Soc.* **2006**, *128*, 7505-7509.
[18] D. Pan, C. Guo, K. Luo, Z. Gu, *Chin. J. Chem.* **2014**, *32*, 27-36.
[19] Y. Zhang, J. Chen, C. Xiao, M. Li, H. Tian, X. Chen, *Biomacromolecules* **2013**, *14*, 4289-4300.
[20] C. Fornaguera, S. Grijalvo, M. Galán, E. Fuentes-Paniagua, F. J. de la Mata, R. Gómez, R. Eritja, G. Calderó, C. Solans, *Int. J. Pharm.* **2015**, *478*, 113-123.
[21] F. Tang, L. Li, D. Chen, *Adv. Mater.* **2012**, *24*, 1504-1534.
[22] M. Colilla, B. González, M. Vallet-Regí, *Biomater. Sci.* **2013**, *1*, 114-134.
[23] D. R. Radu, C.-Y. Lai, K. Jeftinija, E. W. Rowe, S. Jeftinija, V. S.-Y. Lin, *J. Am. Chem. Soc.* **2004**, *126*, 13216-13217.
[24] H. Meng, W. X. Mai, H. Zhang, M. Xue, T. Xia, S. Lin, X. Wang, Y. Zhao, Z. Ji, J. I. Zink, A. E. Nel, *ACS Nano* **2013**, *7*, 994-1005.
[25] M.-H. Kim, H.-K. Na, Y.-K. Kim, S.-R. Ryoo, H. S. Cho, K. E. Lee, H. Jeon, R. Ryoo, D.-H. Min, *ACS Nano* **2011**, *5*, 3568-3576.
[26] F. Gao, P. Botella, A. Corma, J. Blesa, L. Dong, *J. Phys. Chem. B* **2009**, *113*, 1796-1804.
[27] S. B. Hartono, W. Gu, F. Kleitz, J. Liu, L. He, A. P. J. Middelberg, C. Yu, G. Q. (Max) Lu, S. Z. Qiao, *ACS Nano* **2012**, *6*, 2104-2117.
[28] D. Niu, Z. Liu, Y. Li, X. Luo, J. Zhang, J. Gong, J. Shi, *Adv. Mater.* **2014**, *26*, 4947-4953.
[29] X. Huang, Z. Tao, Jr., J. C. Praskavich, A. Goswami, J. F. Al-Sharab, T. Minko, V. Polshettiwar, T. Asefa, *Langmuir* **2014**, *30*, 10886-10898.
[30] E. Fuentes-Paniagua, C. E. Peña-González, M. Galán, R. Gómez, F. J. de la Mata, J. Sánchez-Nieves, *Organometallics* **2013**, *32*, 1789-1796.
[31] M. Galán, E. Fuentes-Paniagua, F. J. de la Mata, R. Gómez, *Organometallics* **2014**, *33*, 3977-3989.
[32] Y.-S. Lin, C.-P. Tsai, H.-Y. Huang, C.-T. Kuo, Y. Hung, D.-M. Huang, Y.-C. Chen, C.-Y. Mou, *Chem. Mater.* **2005**, *17*, 4570-4573.
[33] I. Slowing, B. G. Trewyn, V. S.-Y. Lin, *J. Am. Chem. Soc.* **2006**, *128*, 14792-14793.
[34] J. Lu, M. Liong, J. I. Zink, F. Tamanoi, *Small* **2007**, *3*, 1341-1346.
[35] M. H. Lim, A. Stein, *Chem. Mater.* **1999**, *11*, 3285-3295.
[36] L. T. Zhuravlev, *Colloids and Surfaces A: Physicochem. Eng. Aspects* **2000**, *173*, 1-38.
[37] F. de Juan, E. Ruiz-Hitzky, *Adv. Mater.* **2000**, *12*, 430-432.
[38] J. Kecht, A. Schlossbauer, T. Bein, *Chem. Mater.* **2008**, *20*, 7207-7214.
[39] B. González, M. Colilla, C. López de Laorden, M. Vallet-Regí, *J. Mater. Chem.* **2009**, *19*, 9012-9024.
[40] Y. Vida, M. I. Montañez, D. Collado, F. Najera, A. Ariza, M. Blanca, M. J. Torres, C. Mayorga, E. Perez-Inestrosa, *J. Mater. Chem. B* **2013**, *1*, 3044-3050.
[41] V. A. Kabanov, A. B. Zezin, V. B. Rogacheva, Zh. G. Gulyaeva, M. F. Zansochova, J. G. H. Joosten, J. Brackman, *Macromolecules* **1998**, *31*, 5142-5144.
[42] X. Huang, N. Hauptmann, D. Appelhans, P. Formanek, S. Frank, S. Kaskel, A. Temme, B. Voit, *Small* **2012**, *8*, 3579-3583.
[43] J.-T. Sun, J.-G. Piao, L.-H. Wang, M. Javed, C.-Y. Hong, C.-Y. Pan, *Macromol. Rapid Commun.* **2013**, *34*, 1387-1394.
[44] J. M. Rosenholm, C. Sahlgren, M. Lindén, *Nanoscale* **2010**, *2*, 1870-1883.
[45] I. I. Slowing, B. G. Trewyn, V. S.-Y. Lin, *J. Am. Chem. Soc.* **2006**, *128*, 14792-14793.
[46] J. M. Rosenholm, A. Meinander, E. Peuhu, R. Niemi, J. E. Eriksson, C. Sahlgren, M. Lindén, *ACS Nano* **2009**, *3*, 197-206.
[47] M. J. Serramía, S. Álvarez, E. Fuentes-Paniagua, M. I. Clemente, J. Sánchez-Nieves, R. Gómez, J. de la Mata, M. A. Muñoz-Fernández, *J. Control. Release* **2015**, *200*, 60-70.
[48] I. I. Slowing, J. L. Vivero-Escoto, Y. Zhao, K. Kandel, C. Peeraphatdit, B. G. Trewyn, V. S.-Y. Lin, *Small* **2011**, *7*, 1526-1532.

Entry for the Table of Contents

FULL PAPER

Carbosilane dendrons of second and third generation, with ammonium or tertiary amine groups as peripheral groups, have been prepared and following different strategies have been grafted outside mesoporous silica nanoparticles. The hybrid nanosystem functionalized with the third generation of neutral carbosilane dendron is able to transport single oligonucleotide strands into cells, representing a novel nonviral vector.

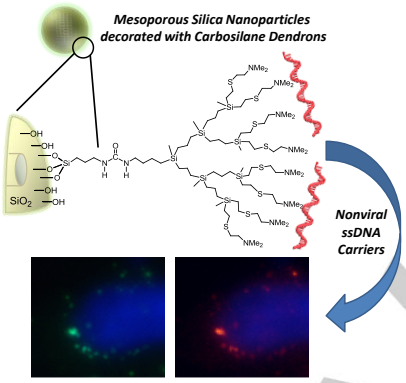

Ángel Martínez, Elena Fuentes-Paniagua, Alejandro Baeza, Javier Sánchez-Nieves, Mónica Cicuéndez, Rafael Gómez, F. Javier de la Mata, Blanca González,* María Vallet-Regí**

Page No. – Page No.

Mesoporous Silica Nanoparticles Decorated with Carbosilane Dendrons as Novel Nonviral Oligonucleotides Delivery Carriers